Monthly Notices of the ROYAL ASTRONOMICAL SOCIETY

MNRAS **522,** 312–318 (2023) https://doi.org/10.1093/mnras/stad990
Advance Access publication 2023 April 4

Expansion and line-binned opacities of samarium ions for the analysis of early kilonova emission from neutron star mergers

H. Carvajal Gallego,[1] J. Deprince,[1,2] P. Palmeri [1] and P. Quinet [1,3]★

[1] *Physique Atomique et Astrophysique, Université de Mons, B-7000 Mons, Belgium*
[2] *Institut d'Astronomie et d'Astrophysique, Université Libre de Bruxelles, B-1050 Brussels, Belgium*
[3] *IPNAS, Université de Liège, Sart Tilman, B-4000 Liège, Belgium*

Accepted 2023 March 30. Received 2023 March 9; in original form 2023 January 17

ABSTRACT

Opacity calculations performed within the expansion and the line-binned formalisms are reported for Sm V–X ions in this paper. These were determined by means of new large-scale atomic structure and radiative rate computations carried out using the pseudo-relativistic Hartree-Fock (HFR) method from which energy levels, wavelengths, and oscillator strengths were deduced for more than 100 millions of spectral lines in the considered samarium ions. In the absence of any experimental data, the reliability of HFR results was roughly estimated by comparison with those obtained with an independent theoretical approach, namely the fully relativistic multiconfiguration Dirac-Hartree-Fock method, in Sm VI and Sm VII. The opacities were estimated for typical conditions corresponding to early phases of kilonovae following neutron star mergers, i.e. for a density $\rho = 10^{-10}$ g cm^{-3}, a time after the merger $t = 0.1$ day and temperatures ranging from 25 000 to 70 000 K. In addition, the atomic calculations allowed us to establish the ground level for each of the Sm ions considered (still unknown until now), as well as reliable partition functions that are crucial for the determination of the ionization balance by solving the Saha equation and for accurate opacity calculations.

Key words: atomic data – atomic processes – opacity – neutron star mergers.

1 INTRODUCTION

In continuation of our recent works focused on new calculations of atomic parameters and relative opacities for the first five lanthanide elements, between La and Pm, in charge states from V to X (Carvajal Gallego et al. 2022a, b, 2023a), this paper is dedicated to samarium ions from Sm V to Sm X. It is indeed now confirmed that such heavy elements are abundantly produced by rapid neutron capture (*r*-process) nucleosynthesis in neutron star mergers (Kasen et al. 2017; Domoto et al. 2022) and, due to their rich spectra containing a large amount of lines, they strongly contribute to the opacities affecting the electromagnetic signals emitted by the kilonovae (see e.g. Tanaka et al. 2018).

As these opacities constitute parameters of paramount importance for the study of kilonovae, in particular with regard to the light curves, their calculations are currently the subject of many investigations. For this purpose, the determination of atomic data (energy levels, wavelengths, oscillator strengths) is necessary for as many radiative transitions as possible in all trans-iron atoms in their various ionization stages.

As far as the lanthanides are concerned, most of the atomic calculations relevant for kilonova opacity determination published until now were focused on the first ionization degrees, typically from I to IV. Among these works, we will mention here those related to Nd II–IV (Gaigalas et al. 2019), Er III (Gaigalas et al. 2020), Pr–Gd II (Radžiūtė et al. 2020), Tb–Yb II (Radžiūtė et al. 2021) Ce II–IV (Carvajal Gallego, Palmeri & Quinet 2021), and Ce IV (Rynkun et al. 2022). Line-binned opacities were also reported by Fontes et al. (2020) for all lanthanide atoms from neutral (I) to trebly ionized (IV) species. For higher ionization stages, in addition to our recent investigations mentioned above concerning La–Pm V–X ions (Carvajal Gallego et al. 2022a, b, 2023a), expansion opacity calculations were carried out for three selected lanthanides, namely Nd, Sm and Eu, between 4 and 10 times ionized (V–XI) by Banerjee et al. (2022).

In this paper, large-scale atomic structure calculations were performed in Sm V–X ions using the pseudorelativistic Hartree-Fock (HFR) method giving rise to the determination of spectroscopic parameters for millions of lines in these ions. A comparison with radiativedata obtained with the multiconfiguration Dirac-Hartree-Fock (MCDHF) method for two selected ions, Sm VI and Sm VII, allowed us to roughly estimate the accuracy of the results. The corresponding opacities were then computed within the expansion and line-binned formalisms for different kilonova temperatures, i.e. $T = 25\,000$, 42 000, 50 000, and 70 000 K.

2 ATOMIC DATA CALCULATIONS

2.1 HFR method

The main method used to calculate the atomic structures and radiative parameters in Sm V–X ions was the HFR approach described by Cowan (1981). In each of the considered ions, configuration interac-

★ E-mail: pascal.quinet@umons.ac.be

tions were explicitly introduced in multiconfigurational expansions taking into account the electronic correlation outside a Pd-like ionic core with 46 electrons filling all subshells from 1s to 4d. Outside this ionic core, the remaining k electrons (with k = 12, 11, 10, 9, 8, and 7 for Sm V, VI, VII, VIII, IX and X, respectively) were assumed to occupy mainly the 4f, 5s, and 5p subshells while allowing some single and double excitations towards more excited valence nl orbitals, with $n \leq 8$ and $l \leq 4$. More precisely, for each ion, the following configurations were included in the HFR calculations:

(i) Sm V: $5s^25p^64f^4 + 5s^25p^54f^5 + 5s^25p^64f^25d^2 + 5s^25p^64f^26s^2 + 5s^25p^64f^26p^2 + 5s^25p^64f^25d6s + 5s^25p^64f^3nf$ (n = 5–8) $+ 5s^25p^64f^3np$ (n = 6–8) $+ 5s5p^64f^4nd$ (n = 5–8) $+ 5s5p^64f^4ns$ (n = 6–8) $+ 5s^25p^65d^3nd$ (n = 6–8) $+ 5s^25p^65d^3ns$ (n = 6–8) (even parity) and $5s^25p^65d^3np$ (n = 6–8) $+ 5s^25p^65d^3nf$ (n = 5–8) $+ 5s^25p^64f^3ns$ (n = 6–8) $+ 5s^25p^64f^3nd$ (n = 5–8) $+ 5s^25p^64f^3ng$ (n = 5–8) $+ 5s^25p^54f^45d + 5s^25p^54f^46s + 5s5p^64f^4np$ (n = 6–8) $+ 5s^25p^64f^25d6p$ (odd parity)

(ii) Sm VI: $5s^25p^64f^3 + 5s^25p^54f^4 + 5s^25p^54f^36p + 5s^25p^64f^2nf$ (n = 5–8) $+ 5s^25p^64f^2np$ (n = 6–8) $+ 5s5p^64f^3nd$ (n = 5–8) $+ 5s5p^64f^3ns$ (n = 6–8) $+ 5s^25p^65d^2np$ (n = 6–8) $+ 5s^25p^65d^2nf$ (n = 5–8) (odd parity) and $5s^25p^65d^3 + 5s^25p^54f^35d + 5s^25p^54f^3ns$ (n = 6–7) $+ 5s^25p^65d^2nd$ (n = 6–8) $+ 5s^25p^65d^2ns$ (n = 6–8) $+ 5s^25p^64f^2ns$ (n = 6–8) $+ 5s^25p^64f^2nd$ (n = 5–8) $+ 5s^25p^64f^2ng$ (n = 5–8) $+ 5s5p^64f^4 + 5s5p^64f^3np$ (n = 6–8) (even parity)

(iii) Sm VII: $5s^25p^54f^3 + 5s^25p^64f^2 + 5s^25p^64fnf$ (n = 5–8) $+ 5s^25p^64fnp$ (n = 6–8) $+ 5s^25p^44f^36p + 5s^25p^65d^2 + 5s^25p^65dnd$ (n = 6–8) $+ 5s^25p^66s^2 + 5s^25p^65dns$ (n = 6–8) $+ 5s5p^64f^2nd$ (n = 5–8) $+ 5s5p^64f^2ns$ (n = 6–8) (even parity) and $5s^25p^44f^35d + 5s^25p^44f^3ns$ (n = 6–7) $+ 5s^25p^64fns$ (n = 6–8) $+ 5s^25p^64fnd$ (n = 5–8) $+ 5s^25p^64fng$ (n = 5–8) $+ 5s^25p^65dnp$ (n = 6–8) $+ 5s^25p^65dnf$ (n = 5–8) $+ 5s^25p^54f^25d + 5s^25p^54f^26s + 5s^25p^55d^3 + 5s5p^64f^3 + 5s5p^64f^2np$ (n = 6–8) (odd parity)

(iv) Sm VIII: $5s^25p^44f^3 + 5s^25p^54f^2 + 5s^25p^55d^2 + 5s^25p^56s^2 + 5s^25p^34f^4 + 5s^25p^34f^36p + 5s^25p^55dns$ (n = 6–8) $+ 5s^25p^54fnp$ (n = 6–8) $+ 5s^25p^54fnf$ (n = 5–8) $+ 5s^25p^6np$ (n = 6–8) $+ 5s^25p^6nf$ (n = 4–8) $+ 5s5p^64fnd$ (n = 5–8) $+ 5s5p^64fns$ (n = 6–8) $+ 5p^64f^3$ (odd parity) and $5s^25p^44f^2nd$ (n = 5–6) $+ 5s^25p^44f^26s + 5s^25p^6ns$ (n = 6–8) $+ 5s^25p^6nd$ (n = 5–8) $+ 5s^25p^6ng$ (n = 5–8) $+ 5s^25p^34f^35d + 5s^25p^34f^3ns$ (n = 6–7) $+ 5s^25p^54fns$ (n = 6–8) $+ 5s^25p^54fnd$ (n = 5–8) $+ 5s5p^64fnp$ (n = 6–8) $+ 5s5p^64fnf$ (n = 5–8) $+ 5s5p^64f^2 + 5p^64f^25d$ (even parity)

(v) Sm IX: $5s^25p^34f^3 + 5s^25p^45d^2 + 5s^25p^46s^2 + 5s^25p^44f^2 + 5s^25p^24f^36p + 5s^25p^45d6s + 5s^25p^24f^4 + 5s^25p^35d^24f + 5s^25p^6 + 5s^25p^5np$ (n = 6–8) $+ 5s^25p^5nf$ (n = 4–8) $+ 5s5p^6ns$ (n = 6–8) $+ 5s5p^6nd$ (n = 5–8) $+ 5s5p^54fns$ (n = 6–8) $+ 5s5p^54fnd$ (n = 5–8) $+ 5p^54f^3 + 5p^64f^2$ (even parity) and $5s^25p^24f^35d + 5s^25p^24f^3ns$ (n = 6–7) $+ 5s^25p^34f^26s + 5s^25p^34f^25d + 5s^25p^5ns$ (n = 6–8) $+ 5s^25p^5nd$ (n = 5–8) $+ 5s^25p^5ng$ (n = 5–8) $+ 5s^25p^44f5d + 5s^25p^44f6s + 5s^25p^35d^3 + 5s5p^6np$ (n = 6–8) $+ 5s5p^6nf$ (n = 4–8) $+ 5s5p^54f^2 + 5s5p^54fnp$ (n = 6–8) $+ 5p^54f^25d + 5p^64f5d$ (odd parity)

(vi) Sm X: $5s^25p^24f^3 + 5s^25p^4nf$ (n = 4–8) $+ 5s^25p4f^36p + 5s^25p^5 + 5s^25p^4np$ (n = 6–8) $+ 5s^25p^34f^2 + 5s^25p^35d^2 + 5s^25p^36s^2 + 5s^25p^35d6s + 5s5p^5nd$ (n = 5–8) $+ 5s5p^5ns$ (n = 6–8) $+ 5p^44f^3 + 5p^54f^2 + 5p^64f + 5s5p^44fnd$ (n = 5–8) $+ 5s5p^44fns$ (n = 6–8) (odd parity) and $5s^25p4f^3nd$ (n = 5–6) $+ 5s^25p4f^3ns$ (n = 6–7) $+ 5s^25p^24f^2nd$ (n = 5–6) $+ 5s^25p^24f^26s + 5s^25p^4ns$ (n = 6–8) $+ 5s^25p^4nd$ (n = 5–8) $+ 5s^25p^4ng$ (n = 5–8) $+ 5s^25p^34f5d + 5s^25p^34f6s + 5s^25p^25d^3 + 5s5p^6 + 5s5p^5np$ (n = 6–8) $+ 5s5p^5nf$ (n = 4–8) $+ 5s5p^44f^2 + 5s5p^44fnp$ (n = 6–8) $+ 5p^65d + 5p^44f^25d + 5p^54f5d$ (even parity)

In addition, in order to estimate the contribution of Sm XI in terms of the ionization balance for the highest temperature considered in our opacity calculations, i.e. T = 70 000 K, more limited HFR computations were also performed in this ion with the same configurations as those included in the physical model of Banerjee et al. (2022), namely $5p4f^3$, $4f^36p$, $5p^24f^2$ and $4f^35d$, $4f^36s$, $4f^37s$ configurations in the even and odd parities, respectively.

As no experimental data is available for these ions, no semi-empirical adjustment of the radial parameters was possible. However, all Slater integrals (F^k, G^k, R^k) were scaled down by a factor of 0.90 as suggested by Cowan (1981) to make a rough allowance for the cumulative effect of the infinity of small perturbations caused by configurations not explicitly included in the HFR models.

2.2 Fully relativistic MCDHF method

In order to evaluate the accuracy of the HFR results obtained in this work, we also performed atomic structure calculations using the MCDHF approach developed by Grant (2007) and Froese Fischer et al. (2016) with the latest version of the General Relativistic Atomic Structure Program (GRASP), i.e. GRASP2018 (Froese Fischer et al. 2019). Two samarium ions were selected for this purpose, namely Sm VI and Sm VII. In each of these ions, a multireference (MR) was chosen to include the configurations between which the radiative transitions were computed. Then valence–valence (VV) and core–valence (CV) correlations were taken into account by adding single and double (SD) excitations involving only valence electrons (i.e. outside the Pd-like $4d^{10}$ core) on one hand, and between core and valence electrons, on the other hand.

For Sm VI, the $5s^25p^64f^3$, $5s^25p^64f5d^2$ odd- and $5s^25p^64f^25d$, $5s^25p^65d^3$ even-configurations were included in the MR. The orbitals from 1s to 4f were optimized on the ground configuration while 5d was optimized using all the MR configurations, keeping all other orbitals fixed. Two VV models were built by adding SD excitations from 5s, 5p, 5d, 4f to {5s, 5p, 5d, 5f, 5g} (VV1) and to {6s, 6p, 6d, 6f, 5g} (VV2) active sets, respectively, where {nl, $n'l'$,...} represent the maximum principal quantum number for each azimuthal quantum number. From the latter, a CV model was then built by adding SD excitations from the 4d core orbital to the MR valence orbitals, namely 5s, 5p, 5d, and 4f. This gave rise to a total of 1675493 configuration state functions (CSFs) for both parities.

In the case of Sm VII, the MR was composed of the $5s^25p^54f^3$, $5s^25p^64f^2$, $5s^25p^65d^2$ even- and the $5s^25p^64f5d$, $5s^25p^55d^3$ odd-configurations in which the 1s–4f and 5d orbitals were optimized on the ground configuration and on all MR configurations, respectively. In VV1 and VV2 models, SD excitations from 5s, 5p, 5d, 4f orbitals to the {5s, 5p, 5d, 5f, 5g} and {6s, 6p, 6d, 6f, 5g} active sets were considered. A CV model was then built from VV2 by adding single excitations from 4d to 5s, 5p, 5d, and 4f subshells. This led to a calculation involving 1581536 CSFs if we consider both parities together.

2.3 Atomic structure and radiative parameters

A first result that we could extract from our calculations consists in the establishment of the fundamental level for each samarium ion considered. This information remained unclear until now, the data available at NIST (Kramida et al. 2022) and those published by Kilbane & O'Sullivan (2010) and Banerjee et al. (2022) being

Table 1. Ground configurations and levels of Sm V–X ions.

Ion	Ground configuration				Ground level
	NIST[a]	Kilbane[b]	Banerjee[c]	This work	This work
Sm V	$5p^6 4f^4$	$5p^6 4f^4$	$5p^6 4f^4$	$5p^6 4f^4$	$^5I_4$
Sm VI	$5p^6 4f^3$	$5p^6 4f^3$	$5p^6 4f^3$	$5p^6 4f^3$	$^4I^o_{9/2}$
Sm VII	$5p^4 4f^4$	$5p^6 4f^2$	$5p^5 4f^3$	$5p^5 4f^3$	$^5H_3$
Sm VIII	$5p^3 4f^4$	$5p^5 4f^2$	$5p^4 4f^3$	$5p^4 4f^3$	$^6H^o_{5/2}$
Sm IX	$5p^2 4f^4$	$5p^3 4f^3$	$5p^3 4f^3$	$5p^3 4f^3$	$^7I_4$
Sm X	$5p4f^4$	$5p^2 4f^3$	$5p^2 4f^3$	$5p^2 4f^3$	$^6K^o_{9/2}$

[a]Kramida et al. (2022).
[b]Kilbane & O'Sullivan (2010).
[c]Banerjee et al. (2022).

Table 2. Partition functions of Sm V–X ions.

T (K)	Sm V $g_0 = 9$	Sm VI $g_0 = 10$	Sm VII $g_0 = 7$	Sm VIII $g_0 = 6$	Sm IX $g_0 = 9$	Sm X $g_0 = 10$
5000	22.96	17.93	24.15	32.04	38.82	13.92
10 000	43.64	31.44	66.01	82.08	76.00	24.59
15 000	72.80	48.26	121.27	167.45	142.89	44.27
20 000	108.60	69.36	185.00	292.42	250.41	78.12
25 000	143.38	96.89	253.47	459.51	403.86	128.74
30 000	192.07	133.13	323.82	668.89	603.40	196.06
35 000	242.19	179.50	394.26	918.21	845.45	278.42
40 000	302.97	236.59	464.10	1203.44	1124.38	373.42
45 000	379.51	304.52	533.70	1519.91	1433.90	478.55
50 000	477.15	383.27	604.36	1863.19	1768.03	591.55
55 000	600.96	472.82	678.05	2229.60	2121.63	710.50
60 000	755.45	573.28	757.17	2616.36	2490.61	834.00
65 000	944.44	684.78	844.31	3021.60	2871.94	961.04
70 000	1170.92	807.53	942.01	3444.21	3263.53	1091.03

often in disagreement, in particular for Sm VII, Sm VIII, Sm IX, and Sm X ions. In Table 1, we compare the fundamental configurations obtained from our HFR models with those published previously. We can notice that, for each Sm ion, we confirm the result of Banerjee et al. (2022) and we give in addition the *LS* coupling designation of the ground level.

Another important parameter deduced from our calculations is the partition function. The most accurate determination of this function is indeed crucial for estimating the ionization balance of a plasma at local thermodynamic equilibrium (LTE) and also for calculating the opacities. As a reminder, for an atomic system, the partition function is given by

$$U(T) = \sum_i g_i \mathrm{e}^{-E_i/k_B T}, \quad (1)$$

where E_i represent all the energy levels belonging to the atomic system, with respect to the ground level, g_i are the corresponding statistical weights ($=2J_i + 1$), and k_B is the Boltzmann constant.

It is therefore essential to know as many energy levels as possible to evaluate the partition function of an ion. Since there are no experimental levels available for Sm V–X ions, the only way to proceed is to use the levels predicted by a theoretical approach. By doing this, we obtained the partition functions given in Table 2. The latter were determined with all the energy levels deduced from our HFR calculations, i.e. 31 142 levels for Sm V, 13 006 levels for Sm VI, 14 495 levels for Sm VII, 23015 levels for Sm VIII, 21 432 levels for Sm IX, and 18 852 levels for Sm X. In the same table, the statistical weight of the ground level (g_0) of each ion is also given for comparison. It is indeed worth mentioning that in many astrophysical investigations, $U(T)$ is often replaced by g_0 when energy levels are not available. If this approximation is acceptable for very low temperatures, it is obviously no longer the case when temperature increases, as shown in Table 2 where $U(T)$ and g_0 are very different from each other for the range of temperatures considered, i.e. from 5000 to 70 000 K. The impact of using realistic partition functions in opacity calculations was recently detailed in another paper (Carvajal Gallego et al. 2023b).

Table 3. Number of transitions and ionization potentials used in opacity calculations of Sm V–X ions.

Ion	Number of lines[a]	IP (cm^{-1})[b]
Sm V	17 267 783	505 400
Sm VI	5426 148	700 000
Sm VII	10 245 968	830 000
Sm VIII	30 795 559	955 000
Sm IX	26 651 944	1140 000
Sm X	12 813 888	1276 000

[a]Number of lines included in HFR calculations (this work).
[b]From NIST data base (Kramida et al. 2022).

In the determination of opacities, it is of paramount importance to have radiative data such as wavelengths and oscillator strengths for a very large number of spectral lines. In our work, these latter parameters were computed using the HFR method for all electric dipole transitions with $\log gf > -5$ involving the whole set of energy levels below the ionization potential of each Sm ion. In Table 3, we list the number of calculated transitions and the ionization potentials for Sm V–X ions. It can be noted that a little more than

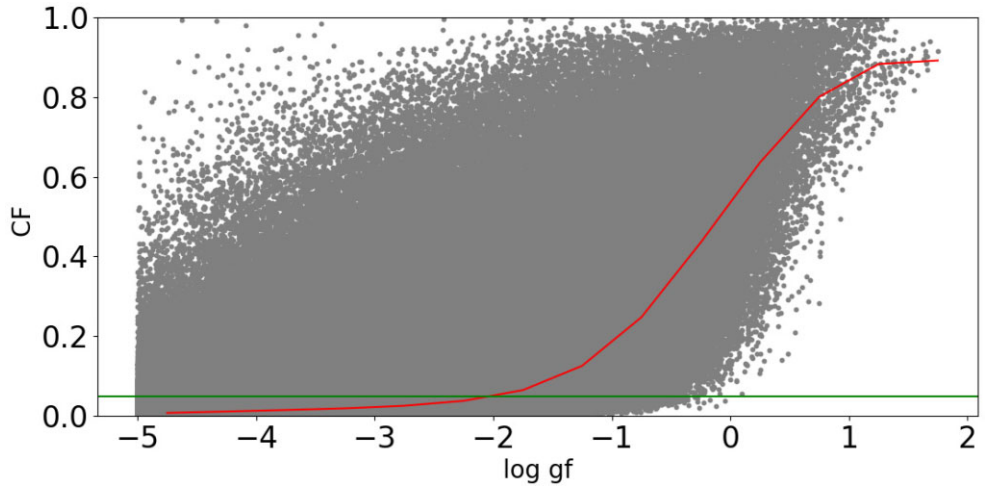

Figure 1. CF as a function of log *gf* for all the Sm VI transitions considered in the present work. The grey dots correspond to the CF values obtained in the HFR calculations for each of the transitions, the red curve corresponds to the evolution of the average CF as a function of the oscillator strength and the green straight line represents CF $= 0.05$.

100 million radiative transitions were calculated if we consider the six ions together. It is of course illusory to evaluate the accuracy of the radiative parameters obtained for such a large number of transitions but an estimate can be made by comparing some of our HFR data with those deduced from the MCDHF calculations also performed in this work for two particular ions, namely Sm VI and Sm VII. When doing such a comparison for transitions involving the ground configurations ($5p^6 4f^3$ for Sm VI and $5p^5 4f^3$ for Sm VII), we found a satisfactory overall agreement between the HFR *gf*-values and the MCDHF data obtained in the Babushkin gauge, the average ratios $gf_{\rm HFR}/gf_{\rm MCDHF}$ being equal to 0.88 and 0.99 for Sm VI and Sm VII, respectively, with a dispersion of the order of a factor of 2 in both cases. For the same transitions, we also noted that the mean differences between the MCDHF oscillator strengths computed within the Babushkin and the Coulomb gauges were about 50 per cent (Sm VI) and 30 per cent (Sm VII). We will therefore make a rough assumption that the HFR oscillator strengths calculated in this work are accurate to within a factor of 2, at least for the most intense lines. Let us specify that the comparison was limited to transitions involving the ground configurations because the latter were used to optimize all the orbitals, from 1s to 4f, in our MCDHF calculations, as described in Section 2.2, and also because it was rather complicated to make an unambiguous correspondence between MCDHF and HFR results for other transitions.

Another way to assess the reliability of our HFR *gf* values is to consider the cancellation factor (CF) associated with each calculated transition, as defined by Cowan (1981). A very small value of this factor (typically smaller than 0.05) indicates that the corresponding oscillator strength might be affected by a larger uncertainty. It was verified in our calculations that, for the vast majority of the strongest transitions (with $\log gf > -2$), contributing the most to the opacity, the CF was greater than 0.05. This is illustrated in Fig. 1 showing the CF values as a function of log *gf* for all the transitions (>5 millions) computed in Sm VI.

3 OPACITY CALCULATIONS

A commonly used approach for computing opacities is based on the expansion formalism. In this approach, the bound–bound opacity is calculated using the expression

$$\kappa_{\rm exp}^{\rm bb}(\lambda) = \frac{1}{\rho c t} \sum_{l \in \Delta\lambda} \frac{\lambda_l}{\Delta\lambda} (1 - {\rm e}^{-\tau_l}), \tag{2}$$

where λ (in Å) is the central wavelength within the region of width $\Delta\lambda$, λ_l are the wavelengths of the lines appearing in this range, τ_l are the corresponding optical depths, c (in cm s^{-1}) is the speed of light, ρ (in g cm^{-3}) is the density of the ejected gas and t (in s) is the elapsed time since ejection.

The optical depth can be expressed using the Sobolev (1960) expression:

$$\tau_l = \frac{\pi {\rm e}^2}{m_{\rm e} c} f_l n_l t \lambda_l, \tag{3}$$

where e (in C) is the elementary charge, $m_{\rm e}$ (in g) is the electron mass, f_l (dimensionless) is the oscillator strength, and n_l (in cm^{-3}) is the density of the lower level of the transition. Since the LTE is assumed in this formalism, n_l can be expressed using the Boltzmann distribution:

$$n_l = \frac{n}{U(T)} g_l {\rm e}^{-E_l/k_{\rm B}T}, \tag{4}$$

where n is the ion density and $U(T)$ is the partition function defined in equation (1).

An alternative method for computing opacities is based on the following line-binned expression (Fontes et al. 2020):

$$\kappa_{\rm bin}^{\rm bb}(\nu) = \frac{\pi {\rm e}^2}{\rho m_{\rm e} c} \sum_l n_l f_l L_l(\nu), \tag{5}$$

where ν is the photon frequency, ρ is the mass density, and $L_l(\nu)$ is the corresponding line profile function. An expression for this discrete opacity is obtained from the continuous opacity by replacing the line profile with $1/\Delta\nu$, i.e.

$$\kappa_{\rm bin}^{\rm bb}(\nu) = \frac{1}{\Delta\nu} \frac{\pi {\rm e}^2}{\rho m_{\rm e} c} \sum_{l \in \Delta\nu} n_l f_l, \tag{6}$$

where $\Delta\nu$ represents the frequency width of a bin.

The form of equation (6) is clearly independent of the expansion time, which is a distinct advantage over methods that assume a homologous flow, such as the expansion-opacity approach. In

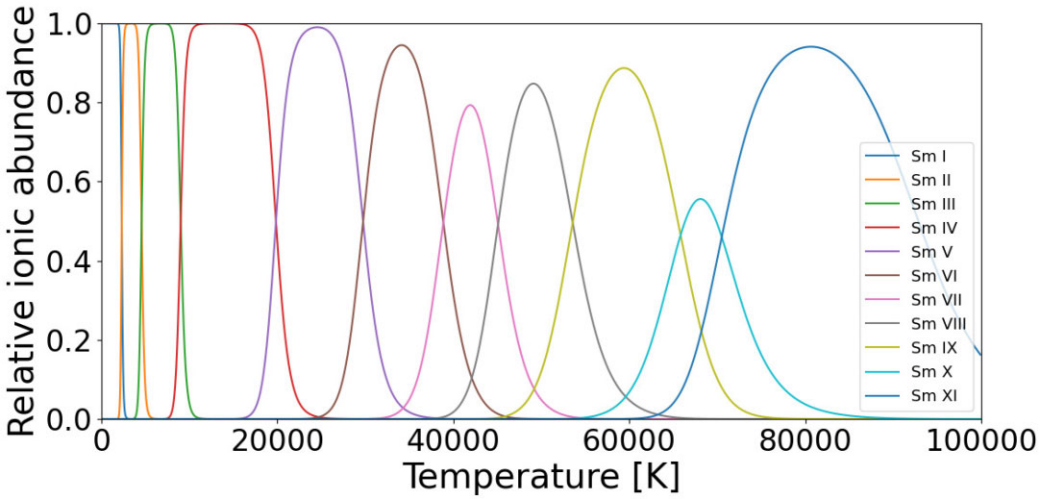

Figure 2. Relative ionic abundances of Sm I–XI ions.

summary, in terms of wavelength, if we consider the optical depth defined by the equation (3), the two approaches give the following relationship:

$$\kappa^{\rm bb} = \frac{1}{\Delta\lambda}\frac{1}{\rho ct}\sum_{l\in\Delta\lambda}\begin{cases}\lambda_l(1-{\rm e}^{-\tau_l}) & \text{for expansion opacity}\\ \lambda_l\tau_l & \text{for line-binned opacity.}\end{cases} \quad (7)$$

Using the whole set of HFR atomic data obtained in this work, the expansion and line-binned opacities were calculated for Sm V–X ions. For these ions, the new partition functions described in Section 2.3, together with partition functions estimated with available energy levels for Sm I–IV taken from the NIST data base (Kramida et al. 2022), were used to solve the Saha equation in order to determine the ionization balance as a function of temperature, as shown in Fig. 2. When looking at the latter, it is clear that the temperature range for which Sm V to Sm X ions show maximum ionic fractions in the plasma extends from 25 000 to 70 000 K. The opacities were thus calculated in this range, considering a density $\rho = 10^{-10}$ g cm^{-3} and a time after merger $t = 0.1$ d, as suggested by Banerjee et al. (2020) for the early phases of kilonovae in which Sm V–X are expected to be present. The wavelength width appearing in equations (2) and (7) was chosen to be $\Delta\lambda = 10$ Å. In Fig. 3, we show the results obtained for four specific temperatures, namely $T = 25\,000$, 42 000, 50 000, and 70 000 K.

In all four cases, our expansion and line-binned opacities are in good agreement in the whole range of wavelengths above 1000 Å. Below this limit, the line-binned opacities are systematically higher (by several orders of magnitude) than the expansion opacities, the discrepancies being more pronounced for the lowest temperature ($T = 25\,000$ K) than for the highest one ($T = 70\,000$ K). Such discrepancies were already highlighted by Fontes et al. (2020) and Banerjee et al. (2022). In the latter work, it was demonstrated that the use of expansion opacities for lanthanides at 0.1 day after neutron star merger should be considered with caution at far UV wavelengths, typically for $\lambda < 2000$ Å, but, in the same paper, it is was also stated that this limit was actually below the detection range of the existing UV instruments like Swift (Roming et al. 2005).

The only previous work with which we can compare our results is the one recently published by Banerjee et al. (2022) who performed expansion opacity calculations for three selected lanthanides, including samarium, up to the ionization XI, using new atomic data obtained from the Hebrew University Lawrence Livermore Atomic Code (HULLAC) developed by Bar-Shalom, Klapisch & Oreg (2001). When comparing our expansion opacity (see fig. 2 of this paper) with the one plotted in fig. 2 of Banerjee et al.'s paper for Sm at $T = 70\,000$ K, we found a good agreement, both curves showing a maximum of $\kappa_{\rm exp} \sim 3 \times 10^2$ cm^2 g^{-1} at $\lambda \sim 500$ Å and a bump of the order of 10 cm^2 g^{-1} at $\lambda \sim 1500$ Å, the opacity slowly decreasing for longer wavelengths to reach, at $\lambda = 10\,000$ Å, values of about 10^{-3} and 10^{-2} cm^2 g^{-1}, in our work and that of Banerjee et al., respectively. This can most likely be explained by the fact that our opacity calculations included more realistic partition functions than in the calculations of Banerjee et al. who usually replace these functions by the statistical weights of the fundamental levels, as discussed in our recent paper (Carvajal Gallego et al. 2023b).

Finally, it is interesting to estimate the sensitivity of opacities obtained in this work to the calculated radiative data. To do so, we assumed that our HFR oscillator strengths were on average accurate to within a factor of 2, as discussed in Section 2.3. From the expressions (7), it is obvious that this uncertainty does not affect the expansion and line-binned opacities in the same way. Indeed, as the line binned opacity is proportional to the sum of the oscillator strengths, an uncertainty of a factor of 2 on the latter implies the same uncertainty on the opacity. On the other hand, the uncertainty affecting the expansion opacity depends on the different f-values involved in the optical depth. More precisely, for a precision of a factor of 2 on the oscillator strengths, the uncertainty on the expansion opacity was estimated as varying between 35 per cent (for $gf = 1$) and a factor of 2 (for $gf = 0.00001$). It thus appears that expansion opacities are overall slightly less sensitive than line-binned opacities with respect to the uncertainties associated with oscillator strength calculations.

4 CONCLUSION

New atomic data were obtained for a large amount of radiative transitions in Sm V–X ions using the HFR theoretical method. The accuracy of oscillator strengths was estimated to be of the order of a factor of 2 by comparison with the results deduced from independent calculations based on the fully relativistic Dirac-Hartree-Fock (MCDHF) approach. Opacities were then computed in expansion and line-binned formalisms for early phase kilonova conditions, i.e. for a density $\rho = 10^{-10}$ g cm^{-3}, a time after the

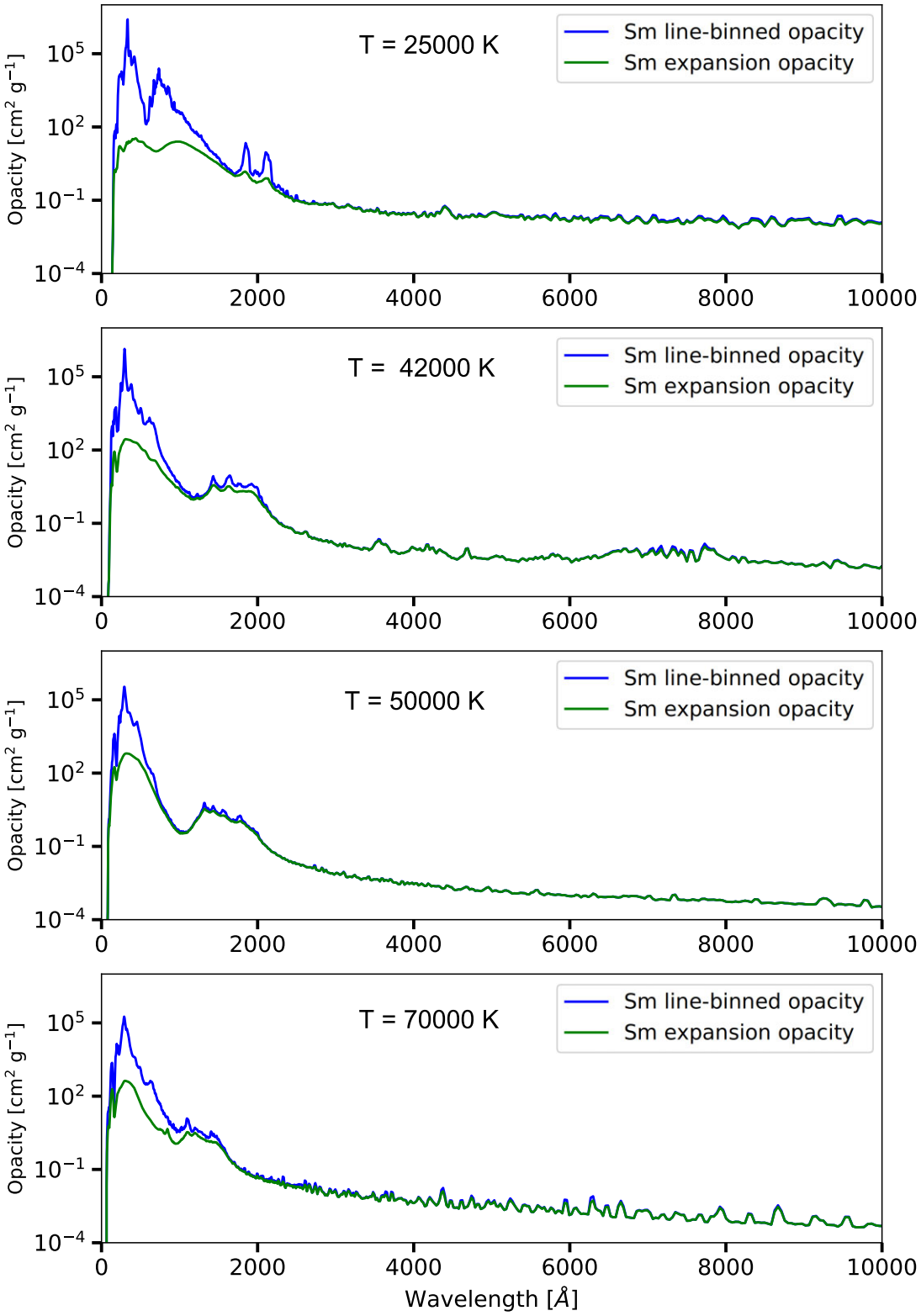

Figure 3. Expansion and line-binned opacities of Sm ions for $T = 25\,000$, 42 000, 50 000, and 70 000 K.

merger $t = 0.1$ d and temperatures ranging from 25 000 to 70 000 K. It was found that both formalisms lead to results in good agreement for wavelengths above 1000 Å, i.e. for the observation range of the current instruments. Reliable partition functions as well as the ground levels in Sm V–X are also reported for the first time in this paper.

ACKNOWLEDGEMENTS

HCG is holder of a FRIA fellowship, while PP and PQ are, respectively, Research Associate and Research Director of the Belgian Fund for Scientific Research F.R.S. - FNRS. This project has received

funding from the FWO and F.R.S. - FNRS under the Excellence of Science (EOS) programme (numbers 0.0228.18 and 0.0004.22). Part of the atomic calculations were made with computational resources provided by the Consortium des Équipements de Calcul Intensif (CECI), funded by the F.R.S. - FNRS under grant no. 2.5020.11 and by the Walloon Region of Belgium.

DATA AVAILABILITY

The data underlying this article will be shared on reasonable request to the corresponding author.

REFERENCES

Banerjee S., Tanaka M., Kato D., Gaigalas G., Kawaguchi K., Domoto N., 2022, ApJ, 934, 117
Banerjee S., Tanaka M., Kawaguchi K., Kato D., Gaigalas G., 2020, ApJ, 901, 29
Bar-Shalom A., Klapisch M., Oreg J., 2001, J. Quant. Spectrosc. Radiat. Transf., 71, 169
Carvajal Gallego H., Berengut J. C., Palmeri P., Quinet P., 2022a, MNRAS, 509, 6138
Carvajal Gallego H., Berengut J. C., Palmeri P., Quinet P., 2022b, MNRAS, 513, 2302
Carvajal Gallego H., Deprince J., Berengut J. C., Palmeri P., Quinet P., 2023a, MNRAS, 518, 332
Carvajal Gallego H., Deprince J., Godefroid M., Goriely S., Palmeri P. Q. P., 2023b, Eur. Phys. J. D., in press (accepted for publication)
Carvajal Gallego H., Palmeri P., Quinet P., 2021, MNRAS, 501, 1440
Cowan R. D., 1981, The Theory of Atomic Structure and Spectra. California Univ. Press, Berkeley
Domoto N., Tanaka M., Kato D., Kawaguchi K., Hotokezaka K., Wanajo S., 2022, ApJ, 939, 8
Fontes C. J., Fryer C. L., Hungerford A. L., Wollaeger R. T., Korobkin O., 2020, MNRAS, 493, 4143
Froese Fischer C., Gaigalas G., Jönsson P., Bieroń J., 2019, Comput. Phys. Commun., 237, 184
Froese Fischer C., Godefroid M., Brage T., Jönsson P., Gaigalas G., 2016, J. Phys. B: At. Mol. Opt. Phys., 49, 182004
Gaigalas G., Kato D., Rynkun P., Radžiūtė L., Tanaka M., 2019, ApJS, 240, 29
Gaigalas G., Rynkun P., Radžiūtė L., Kato D., Tanaka M., Jönsson P., 2020, ApJS, 248, 13
Grant I. P., 2007, Relativistic Quantum Theory of Atoms and Molecules. Springer, New York (USA)
Kasen D., Metzger B., Barnes J., Quataert E., Ramirez-Ruiz E., 2017, Nature, 551, 80
Kilbane D., O'Sullivan G., 2010, Phys. Rev. A, 82, 062504
Kramida A., Ralchenko Yu., Reader J., NIST ASD Team, 2022, NIST Atomic Spectra Database (ver.5.7.1.). Available online at https://physics.nist.gov/asd (accessed in December 2022)
Radžiūtė L., Gaigalas G., Kato D., Rynkun P., Tanaka M., 2020, ApJS, 248, 17
Radžiūtė L., Gaigalas G., Kato D., Rynkun P., Tanaka M., 2021, ApJS, 257, 29
Roming P. W. A. et al., 2005, Space Sci. Rev., 120, 95
Rynkun P., Banerjee S., Gaigalas G., Tanaka M., Radžiūtė L., Kato D., 2022, A&A, 658, A82
Sobolev V. V., 1960, Moving Envelopes of Stars. Harvard Univ. Press, Cambridge, MA (USA)
Tanaka M., Kato D., Gaigalas G. et al., 2018, ApJ, 852, 109

This paper has been typeset from a TEX/LATEX file prepared by the author.